Single-Beam Integrated Hybrid Optical Pumping Spin Exchange Relaxation Free Magnetometer for Biomedical Applications

Yintao Ma[1, 2], Zhixia Qiao[3], Mingzhi Yu[1, 2], Yanbin Wang[1, 2], Yao Chen[1, 2, 4*], Guoxi Luo[1, 2, 4*], Ping Yang[1, 2, 4], Qijing Lin[1, 2, 4], Libo Zhao[1, 2, 4], Yun Zhang[5], Junjie Sun[5], Guangzhao Qin[5], Zhuangde Jiang[1, 2, 4]

[1]*State Key Laboratory for Manufacturing Systems Engineering, International Joint Laboratory for Micro/Nano Manufacturing and Measurement Technologies, Xi'an Jiaotong University (Yantai) Research Institute for Intelligent Sensing Technology and System, Xi'an Jiaotong University, Xi'an 710049, China*

[2]*School of Mechanical Engineering, Xi'an Jiaotong University, Xi'an 710049, China*

[3]*The Eleventh Research Institute of The Sixth Academy of CASC, Xi'an 710100, China*

[4]*Shandong Laboratory of Yantai Advanced Materials and Green Manufacturing, Yantai 265503, China*

[5]*Brightstone Innovation (Yantai) Research Institute for Micronano Sensing Technology, Yantai 264006, China*

*corresponding authors (E-mail: yaochen@xjtu.edu.cn and luoguoxi@xjtu.edu.cn)

Abstract: An ingenious approach to accomplish the high signal strengthen and relatively homogeneous spin polarization has been presented in hybrid optical pumping SERF atomic magnetometer only utilizing single-beam configuration. We have experimentally demonstrated an approximately 3-fold enhancement of the output signal at the optimal spin polarization by optical pumping the thin vapor due to the same spin evolution behavior of the two different kinds of vapor atoms. Eventually, a measuring sensitivity of 30 fT/Hz$^{1/2}$ has been achieved combined with the homemade differential detection system for attenuating large background offset and suppressing optical power noise. This scheme provides a prospect for the development of ultra-highly sensitive and chip-scale atomic magnetometer for the applications that desire for both high signal-to-noise ratio and uniform spin polarization such as magnetocardiography (MCG) and magnetoencephalography (MEG).

The optically pumped atomic magnetometers utilize the interaction between the spin polarization projection of the polarized alkali vapor atoms and the detection light, which is manifested as a change in the transmitted light intensity of the circularly polarized light[1, 2] or a rotation of the polarization plane of the linearly polarized light[3, 4] to realize an ultra-high sensitivity characterization of the magnetic field. One of the most representative types, the spin-exchange-relaxation-free (SERF) magnetometer owing to elimination of spin exchange collisions relaxation has become the most sensitive magnetic detector to date[5]. And Dang *et al.* has achieved the intrinsic magnetic field noise of 0.16 $fT/Hz^{1/2}$ at 40 Hz using a gradiometer detection arrangement for the measurements of weakly magnetized rock samples[6]. Compared with superconducting quantum interference devices (SQUIDs), SERF atomic magnetometer does not require liquid helium cooling equipment, and have also the extremely prominent advantages of high spatial resolution, flexible wearable configuration, and expedient to chip-integrable fabrication combined with the Nano/Micro Electro-Mechanical Systems (NEMS/MEMS) techniques[7-10].Therefore, they have been the subject of a prospering research direction.

However, there are three majorly constraining, but not irremediable issues that need to be addressed for SERF magnetometer for real-world bio-magnetic imaging applications, (i). expanded spin polarization gradient throughout the whole sensor due to high atomic density; (ii). reduced number of effective atoms due to chip-scale integration; (iii). increased susceptibility to laser power noise. The homogeneous spin polarization is very strongly desired in applying multi-channel atomic magnetometer arrays to bio-magnetic field source imaging measurements, such as MCG and MEG. Realistically, there is a fundamental contradiction between atomic polarization uniformity and alkali metal density number in typical SERF atomic magnetometer configuration. In order to improve signal strengthen, the atomic density will be increased; And on the other hand, the high atomic density would impose a limit on the achievable homogeneous spin polarization. In addition, the optimal experimental condition of magnetic field sensitivity, i.e., electron spin polarization of 50%, is difficult to maintain throughout the entire vapor cell due to strong optical absorption in optically thick media. To ameliorate these problems mentioned above, hybrid optical pumping technique is proposed and employed in atomic magnetometers[11-13] and co-magnetometer[14, 15], which can be accomplished by optical pumping the thin vapor atoms and probing the thick atoms utilizing two independent orthogonal laser beams. At the same time, in response to these problems, Yosuke Ito's research group at Kyoto University has made a detailed theoretical modeling analysis and experimental verification with the two orthogonal pump-probe beams configuration[16-19], and came to the conclusion that optically thick alkali metal atoms can also achieve the uniform spin polarization in K and Rb vapor atoms hybrid cell. Li *et al*. constructed a K-Rb hybrid pumping magnetometer and proposed suppression method of light shift and optimization of density ratio by conventionally optical pumping the thin K atoms and probing the thick Rb atoms[20, 21].

Herein, we demonstrate a hybrid optical pumping SERF atomic magnetometer only exploiting single-beam arrangement for both pumping and probing electronic spin polarization. The spin polarization of optically thin vapor atoms from pumping beam can be transferred to optically thick atoms by fast spin exchange collisions process. More importantly, the two different types of alkali atoms can be approximately regarded as the same one from the perspective of steady-state solution of the Bloch equation. Therefore, both high signal strength due to increased atomic density as well as homogeneous spin polarization caused by the optical pumping the less density atoms can be accomplished based on the proposed methodology. At the same time, the optical power noise and background offset can be greatly suppressed by means of subtracting the light intensities before and after the vapor cell using the homemade differential detection system. The developed approach paves the way toward chip-scale integration of ultra-sensitive multi-channel magnetometer arrays for the applications of high-spatial resolution magnetic source imaging.

Similar to the spin dynamics of single-species alkali atomic magnetometers, the atomic spin evolution process under fast spin exchange rate can be also modelled by density matrix in hybrid pumping atomic magnetometer. However, the atomic spin precession is slow enough when atoms are operated under the SERF regime that the evolution behavior of spin polarization $\boldsymbol{P}$ can be described by the Bloch equation[22, 23]:

$$\frac{d\boldsymbol{P}_{Cs}}{dt} = \frac{1}{q_{Cs}}[\gamma^e \boldsymbol{P}_{Cs} \times \boldsymbol{B} + R_{op}\boldsymbol{s} + R_{ex}^{Rb-Cs}\boldsymbol{P}_{Rb} - (\Gamma_{Cs} + R + R_{ex}^{Rb-Cs})\boldsymbol{P}_{Cs}] \tag{1}$$

$$\frac{d\boldsymbol{P}_{Rb}}{dt} = \frac{1}{q_{Rb}}[\gamma^e \boldsymbol{P}_{Rb} \times \boldsymbol{B} + R_{ex}^{Cs-Rb}\boldsymbol{P}_{Cs} - (\Gamma_{Rb} + R_{ex}^{Cs-Rb})\boldsymbol{P}_{Rb}] \tag{2}$$

where the subscript *Cs* and *Rb* represent different atom types, q is the nuclear slowing-down factor depending on alkali electron polarization, γ^e is the gyromagnetic ratio of the electron, R_{op} is the optical pumping rate of circularly polarized light, $\boldsymbol{B}$ is the applied magnetic field, $\boldsymbol{s}$ is the optical pumping vector, Γ is spin relaxation rate except optical pumping and R_{ex} is the spin exchange collisions rate. The equilibrium spin polarizations without magnetic field of equation (1) and equation (2) for Cs and Rb vapor atoms are given by:

$$P_0^{Cs} = \frac{(\Gamma_{Rb} + R_{ex}^{Cs-Rb})R_{op}}{\left(\Gamma_{Cs} + R_{op} + R_{ex}^{Rb-Cs}\right)\left(\Gamma_{Rb} + R_{ex}^{Cs-Rb}\right) - R_{ex}^{Cs-Rb}R_{ex}^{Rb-Cs}} \quad (3)$$

$$P_0^{Rb} = \frac{R_{ex}^{Cs-Rb}R_{op}}{\left(\Gamma_{Cs} + R_{op} + R_{ex}^{Rb-Cs}\right)\left(\Gamma_{Rb} + R_{ex}^{Cs-Rb}\right) - R_{ex}^{Cs-Rb}R_{ex}^{Rb-Cs}} \quad (4)$$

An interesting phenomenon that the steady-state solutions are approximately equal can be found when $R_{ex} >> \Gamma_{Rb}$, which would be readily satisfied in SERF magnetometer. Similarly, in the case of applying external magnetic field, the same conclusion can be also drawn, that is, $P_{x\text{-}Cs} \approx P_{x\text{-}Rb}$, $P_{y\text{-}Cs} \approx P_{y\text{-}Rb}$, $P_{z\text{-}Cs} \approx P_{z\text{-}Rb}$, thus the two different kinds of alkali atoms (i.e., thin Cs atoms and thick Rb atoms) can be regarded as the same one. In other word, although the thin Cs vapor atoms are optically pumped, the optically thick Rb atoms dominate the desired results. Ultimately, the expected experimental results, including high signal strength and homogeneous spin polarization, can be accomplished. At the same time, the required stronger optical pumping intensity in the hybrid pumping magnetometer is about $I_{H\text{-}Laser} \approx I_{S\text{-}Laser}/f$, which ascribes to the transfer of spin polarization between the two alkali atoms. And the reduction in pumping light at any location z in the direction of light propagation is given by:

$$\frac{dI_{H-Laser}(z)}{dz} = -n_{Cs}\sigma(\nu)I_{H-Laser}(z)[1-P_Z] \quad (5)$$

where f is density ratio of Cs to Rb density number, n_{Cs} is the Cs density number, $\sigma(\nu)$ is the photon absorption cross section, P_z is the spin polarization along the direction of laser propagation, $I_{H\text{-}Laser}$ and $I_{S\text{-}Laser}$ are the optical intensities required for hybrid pumping and single-species alkali atoms magnetometer, respectively. The thin Cs vapor atoms are optically pumped, the spin polarizability therefore remains substantially homogeneous across the laser propagation path. The solution to equation (5) can be obtained by:

$$I_{H-Laserout0} = \frac{n_{Rb}I_{S-Laser}}{n_{Cs}} e^{-n_{Cs}\sigma(\nu)L[1-P_Z]} \quad (6)$$

Generally, a sinusoidally modulated magnetic field is applied perpendicular to the direction of pumping light in single-beam magnetometer, and the optimal spin polarization is 50%, and the output light intensity is:

$$
\begin{aligned}
I^{*}_{H-Laserout} &= \frac{n_{Rb} I_{S-Laser}}{n_{Cs}} e^{-n_{Cs}\sigma(\nu)L[1-P_Z-\delta P]} \\
&= I_{H-Laserout0} + \frac{n_{Rb} I_{S-Laser}}{n_{Cs}} n_{Cs}\sigma(\nu)L\delta P e^{-[1-P_Z]n_{Cs}\sigma(\nu)L}
\end{aligned}
\tag{7}
$$

where $I_{H\text{-}Laser0}$ is the constant background offset signal after passing through the vapor cell, L is the length of the vapor cell, δP is the change spin polarization caused by the modulation magnetic field. After differential detection of the two photodetectors before and after the vapor cell, the $I_{H\text{-}Laser0}$ offset signal can be attenuated as low as 500 nA, and laser amplitude noise and other common mode noise can be also greatly suppressed at the same time. Considering the absence of applied magnetic field, the change of output intensity δI is given by:

$$
\delta I = \frac{n_{Rb} I_{S-Laser}}{n_{Cs}} n_{Cs}\sigma(\nu)L\delta P e^{-.5n_{Cs}\sigma(\nu)L}
\tag{8}
$$

In the hybrid optical pumping experiment, the required pumping light intensity becomes stronger, and then the output signal is markedly enhanced. More importantly, the mark of availably homogeneous spin polarization also hits throughout the entire magnetometer head.

The simplified experimental setup is shown in Figure 1(a). A miniaturized cylindrical vapor cell with the length of 3 mm and diameter of 3 mm is filled with a droplet of the mixture of Cs and Rb, 3 amagat Ne and 50 torr N_2. The Rb is natural abundance which contains 72.2% of ^{85}Rb and 27.8% of ^{87}Rb. The density ratio of Cs and Rb is about 1:3 obtained by the laser absorption spectroscopy technique. And the key sensitive vapor cell is placed in the center of the nested magnetic shields, which is comprised of five μ-metal shields and the innermost Mn-Zn ferrite shield for attenuating the Earth's magnetic field to several nT. The residual magnetic field around the cell is further compensated by homemade high precision tri-axial coils wrapped around a 3D printed Teflon skeleton. The cell is optically heated to a normal operating temperature of 160 °C with the Cs optical depth approximately 2.3 with an additional 1550 nm laser, the process can be accomplished by the optical absorption of filter attached to the cell without introducing any stray field[2, 24].

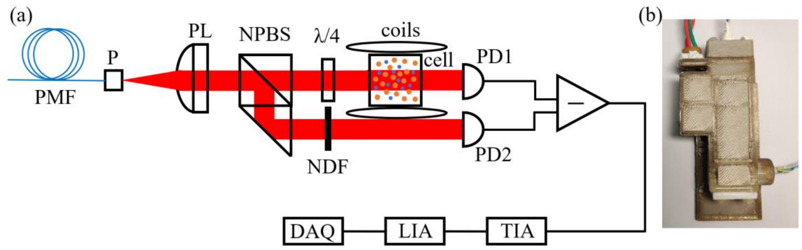

Figure 1. (a) Schematic of the atomic magnetometer. PMF: polarization maintaining fiber; P: fiber coupled port; PL: planoconvex lens; NPBS: non-polarization beam splitter; λ/4: quarter-wave plate; PD: photodiode; NDF: neutral density filter; TIA: transimpedance amplifier; LIA: lock-in amplifier; DAQ: data acquisition system. (b) Sensitive head of the atomic magnetometer.

A distributed-feedback (DFB) laser on-resonance with the center of the Cs atom D1 transition line is coupled to magnetometer head through a single-mode polarization maintaining fiber (PMF). Then the beam is split into two beams by a non-polarization beam splitter (NPBS). One beam is circularly polarized by a quarter-wave plate (λ/4) for optical pumping the thin Cs vapor atoms, and the spin polarization of the thick Rb atoms can be accomplished by spin exchange collisions process with spin polarized Cs atoms. The transmitted beam passing through the vapor cell is received by a silicon photodiode (PD1). Meanwhile, the other beam is treated as a reference beam to realize optical differential detection. Such optical configuration can subtract the light intensity before and after passing through the cell, (i.e., reference beam and measurement beam), and effectively suppress the background offset and common mode noise of the light intensity by carefully controlling the variable neutral density filter (NDF) orientation. The differential signal passes successively through the transimpedance amplifier (TIA) and the lock-in amplifier (LIA), and then is stored and processed by the data acquisition system (DAQ). Figure 1(b) presents the sensitive head of the hybrid optical pumping magnetometer.

The zero-field resonance linewidth under different pumping power density is firstly measured for optimizing the power density [25]. The relationship between power density and resonance linewidth is shown in Figure 2 and can be fitted linearly, from which the corresponding linewidth is 5.4 nT by extrapolation to the zero optical power point, mainly including spin-destruction collisions rate, wall collisions with the bare surface of the cell and other spin relaxation mechanism. The inset in Figure 2 indicates the dispersive zero field magnetic resonance curve under about 50% spin polarization when the incident optical power density is 13.9 mW/cm^2, which is acquired by zero-crossing the transverse scanning magnetic field and recording the output signal of the magnetometer. Then, the experimental result behaves as a dispersive Lorentzian function and the resonance linewidth of the curve is extracted approximately 11 nT corresponding to the total relaxation rate of 1935 s^{-1}.

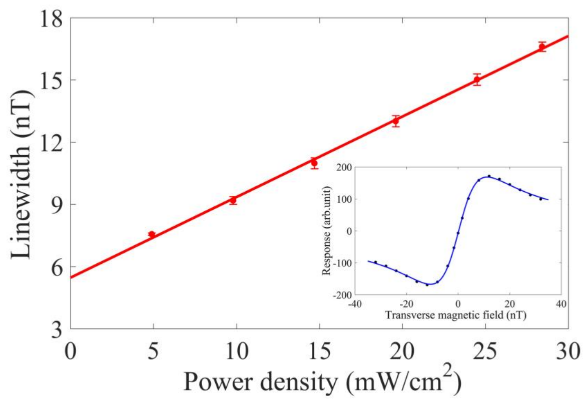

Figure 2. The linear relationship between pumping power density and magnetic resonance linewidth. And the inset is the dispersive response to transverse scanning magnetic field under 50% spin polarization.

To further experimentally demonstrate the enhanced signal intensity in the hybrid optical pumping scheme, a calibration field in the direction perpendicular to pumping beam with the amplitude of 0.8 nTrms and frequency of 30 Hz is applied to the two different types of magnetometer configurations with the same density number of Cs atoms. Figure 3 clearly indicates the dependence of the output signal strength on pumping power density. When the pumping power density is low, the signal amplitude of the single-species Cs atoms magnetometer is higher than that of the hybrid optical pumping scheme. However, the latter output signal increases significantly at high power density. The main reason can be attributed to the spin polarization, where hybrid optical pumping typically requires a higher power density for achieving the same spin polarization, as theoretically analyzes. At smaller pumping power density, the enhanced signal strength is insufficient to compensate for the lower polarization, so the output signal is lower than that of single-species Cs atoms arrangement. As the pumping power increases, the spin polarization of the hybrid optical pumping magnetometer increases faster, a higher output signal can be seen. A near 3-fold enhancement of the output signal strength is eventually achieved in comparison with the single-species Cs atoms magnetometer system under optimal spin polarization of 50%. This phenomenon also reveals that although the hybrid optical pumping scheme leads to a higher signal strength, it also requires higher pumping power density which inevitably brings more serious optical power noise considered as the main noise source in single-beam configuration[1]. Therefore, an optical differential detection strategy is utilized for suppressing the background offset and laser power noise by subtracting the light between the measurement optical path and reference signal after and before the hybrid vapor cell with a homemade differential detection circuit.

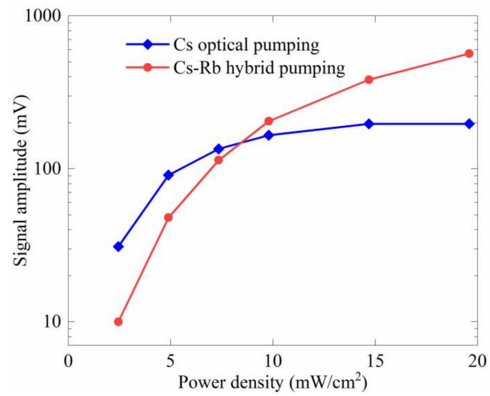

Figure 3. Signal amplitude at a calibration field with an amplitude of 0.8 nTrms and frequency of 30 Hz for single Cs atoms (blue line) and Cs-Rb hybrid optical pumping (red line) magnetometers.

Figure 4 shows the normalized frequency response curve, a manifestation of a first order low pass filter, that the measurement bandwidth of the hybrid pumping magnetometer, i.e., the -3dB bandwidth of frequency response is about 46 Hz. For comparison, the bandwidth of the single-species Cs atoms magnetometer is 115 Hz. The difference in bandwidths is mainly attributable to the fact that in single-beam hybrid optical pumping magnetometer, two different types of atoms can be regarded as the same atom due to the fast spin-exchange collision of Cs and Rb atoms. Therefore, optically thick Rb atoms play a leading role, resulting in reduced resonance linewidth and bandwidth.

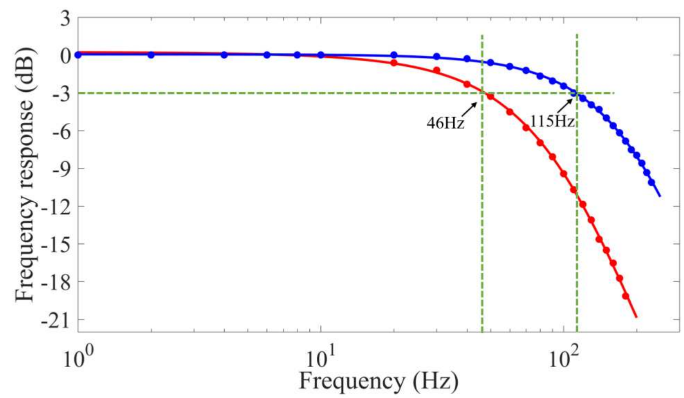

Figure 4. Normalized frequency response curve of two different types magnetometers. The blue curve is single-species Cs atoms magnetometer with the bandwidth of 115 Hz and the red curve represents the proposed hybrid optical pumping magnetometer with the bandwidth of 46 Hz.

Finally, the noise spectral density of the magnetometer at the neighborhood of approximately zero magnetic field with an applied modulation magnetic field in the *X* direction perpendicular to pumping beam direction is presented in the Figure 5. And the modulation amplitude and modulation frequency are 180 nT and 940 Hz, respectively. Eventually, a measuring magnetic field sensitivity of 30 fT/Hz$^{1/2}$ has been achieved in hybrid optical pumping system. An approximately twice the optical power noise suppression effect can be seen by the differential method in our system. Moreover, the electronic noise and dark current noise of the photodetectors can be also obtained by turning off the laser and acquiring the output signal.

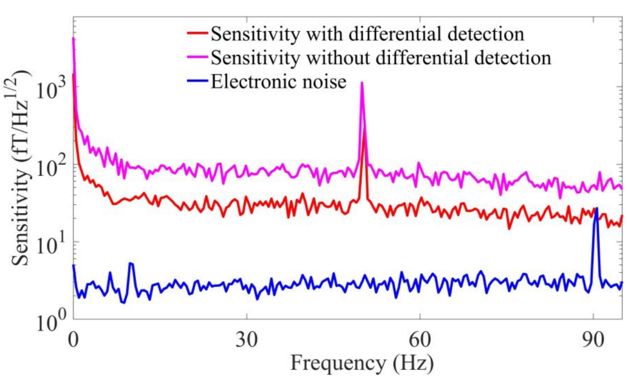

Figure 5. The noise spectral density of the hybrid optical pumping magnetometer with the

sensitivity of 30 fT/Hz$^{1/2}$.

The two essential conditions for realizing SERF regime are low magnetic field strengthen and high atomic density in SERF atomic magnetometer[5, 26, 27]. The former can be satisfied by means of passive magnetic shielding and active magnetic compensation technologies. Generally, heating the vapor cell is the most fashionable method to increase the atomic density, which is proportional to the output signal of the magnetometer[28]. However, the strongly optical absorption by hot vapor atoms would lead to a large and prominent spin polarization gradient throughout the whole sensitive magnetometer head. This phenomenon has become a serious problem in the applications of MCG and MEG. Fortunately, the proposed hybrid optical pumping scheme with single-beam arrangement can effectively ameliorate these problems while maintaining a considerable simplification arrangement. The desired signal strength can be obtained by carefully controlling the density ratio of two different kinds of alkali atoms when fabricating the vapor cell, and incorporating laser power noise suppression techniques such as differential detection or laser power stabilization method, it is expected to achieve fT level and even higher sensitivity as it intends to reach in the such simplified single-beam configuration. The integrated advantages of the proposed single-beam hybrid optical pumping magnetometer are embodied in the following aspects: (i). more homogeneous spin polarization due to optical pumping the thin Cs vapor atoms; (ii). higher signal strength because of the same spin evolution behavior of two different alkali metal atoms; (iii). easier integration of chip-scale atomic magnetometers due to only utilizing a single-beam configuration.

In summary, we have proposed a miniaturized hybrid optical pumping SERF atomic magnetometer only exploiting a single-beam configuration. Compared with the single alkali metal atom magnetometer, a factor of three improvement of the output signal strengthen related to the density ratio has been demonstrated under the same experimental conditions. Furthermore, the developed magnetometer shows a measuring sensitivity of 30 fT/Hz$^{1/2}$ combined with the homemade differential detection system. We are trying to further improve the sensitivity by increasing the density ratio of Rb and Cs atoms painstakingly. The presented approach has an important implication for the development of miniaturized multi-channel magnetometer arrays with high sensitivity and highly uniform spatial polarization for the applications of bio-magnetic field imaging such as MCG and MEG.

Acknowledgments

This work was supported in part by the National Key Research & Development (R&D) Plan (2021YFB2012000), National Natural Science Foundation of China (51890884, U1909221), and the Chongqing Natural Science Basic Research Project (cstc2021jcyj-msxmX0801).

AUTHOR DECLARATIONS

Conflict of Interest

The authors have no conflicts to disclose.

DATA AVAILABILITY

The data that support the findings of this study are available within the article and its supplementary material.

References

1. V. Shah, S. Knappe, P. D. D. Schwindt and J. Kitching, Nat. Photonics. **1** (11), 649-652 (2007).
2. R. Mhaskar, S. Knappe and J. Kitching, Appl. Phys. Lett. **101**, 241105 (2012).
3. M. P. Ledbetter, I. M. Savukov, V. M. Acosta, D. Budker and M. V. Romalis, Phys. Rev. A **77** (3) (2008).
4. S. J. Seltzer and M. V. Romalis, Appl. Phys. Lett. **85** (20), 4804-4806 (2004).
5. J. C. Allred, R. N. Lyman, T. W. Kornack and M. V. Romalis, Phys. Rev. Lett. **89** (13), 130801 (2002).
6. H. B. Dang, A. C. Maloof and M. V. Romalis, Appl. Phys. Lett. **97** (15) (2010).
7. D. Sheng, A. R. Perry, S. P. Krzyzewski, S. Geller, J. Kitching and S. Knappe, Appl. Phys. Lett. **110**, 031106 (2017).
8. E. Boto, N. Holmes, J. Leggett, G. Roberts, V. Shah, S. S. Meyer, L. D. Munoz, K. J. Mullinger, T. M. Tierney, S. Bestmann, G. R. Barnes, R. Bowtell and M. J. Brookes, Nature **555** (7698), 657-661 (2018).
9. G. Liu, J. Tang, Y. Yin, Y. Wang, B. Zhou and B. Han, IEEE Sens. J. **20** (11), 5827-5833 (2020).
10. K. Wang, J. Lu, Y. Yan, J. Tang, M. Ye, K. Yin, Z. Chai, B. Zhou, X. Ning and B. Han, IEEE Sens. J. **22** (3), 2016-2023 (2022).
11. M. V. Romalis, Phys. Rev. Lett. **105** (24), 243001 (2010).
12. W. Li, X. Peng, D. Budker, A. Wickenbrock, B. Pang, R. Zhang and H. Guo, Opt. Lett. **42** (20), 4163-4166 (2017).
13. K. Nishi, Y. Ito and T. Kobayashi, Opt. Express **26** (2), 1988-1996 (2018).
14. J. Fang, Y. Chen, S. Zou, X. Liu, Z. Hu, W. Quan, H. Yuan and M. Ding, Journal of Physics B: Atomic, Molecular and Optical Physics **49** (6) (2016).
15. R. Li, W. Quan, W. Fan, L. Xing and J. Fang, Sensors and Actuators A: Physical **266**, 130-134 (2017).
16. Y. Ito, H. Ohnishi, K. Kamada and T. Kobayashi, IEEE Trans. Magn. **47** (10), 3550-3553 (2011).

17. Y. Ito, H. Ohnishi, K. Kamada and T. Kobayashi, AIP Adv **2** (3) (2012).
18. Y. Ito, H. Ohnishi, K. Kamada and T. Kobayashi, IEEE Trans. Magn. **48** (11), 3715-3718 (2012).
19. Y. Ito, D. Sato, K. Kamada and T. Kobayashi, Opt. Express **24** (14), 15391-15402 (2016).
20. Y. Li, M. Ding, X. Liu, H. Cai, J. Zhao and J. Fang, IEEE Photonics Journal **10** (5), 1-7 (2018).
21. Y. Li, X.-J. Liu, H.-W. Cai, M. Ding and J.-C. Fang, Measurement Science and Technology **30** (1) (2019).
22. J. Fang, T. Wang, H. Zhang, Y. Li and S. Zou, Rev. Sci. Instrum. **85** (12), 123104 (2014).
23. S. Ito, Y. Ito and T. Kobayashi, Opt. Express **27** (6), 8037-8047 (2019).
24. O. Alem, R. Mhaskar, R. Jimenez-Martinez, D. Sheng, J. LeBlanc, L. Trahms, T. Sander, J. Kitching and S. Knappe, Opt. Express **25** (7), 7849-7858 (2017).
25. V. K. Shah and R. T. Wakai, Phys Med Biol **58** (22), 8153-8161 (2013).
26. I. K. Kominis, T. W. Kornack, J. C. Allred and M. V. Romalis, Nature **422** (6932), 596-599 (2003).
27. V. Shah and M. V. Romalis, Phys. Rev. A **80** (1) (2009).
28. M. R. Dmitry Budker, Nat. Phys. **3**, 227–234 (2007).

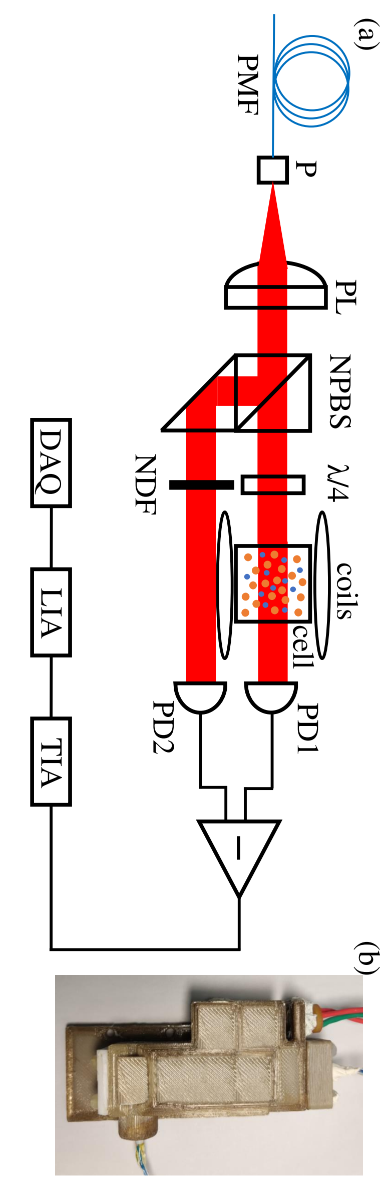
(a)
PMF
P
PL
NPBS
λ/4
coils
cell
NDF
PD1
PD2
−
DAQ
LIA
TIA
(b)

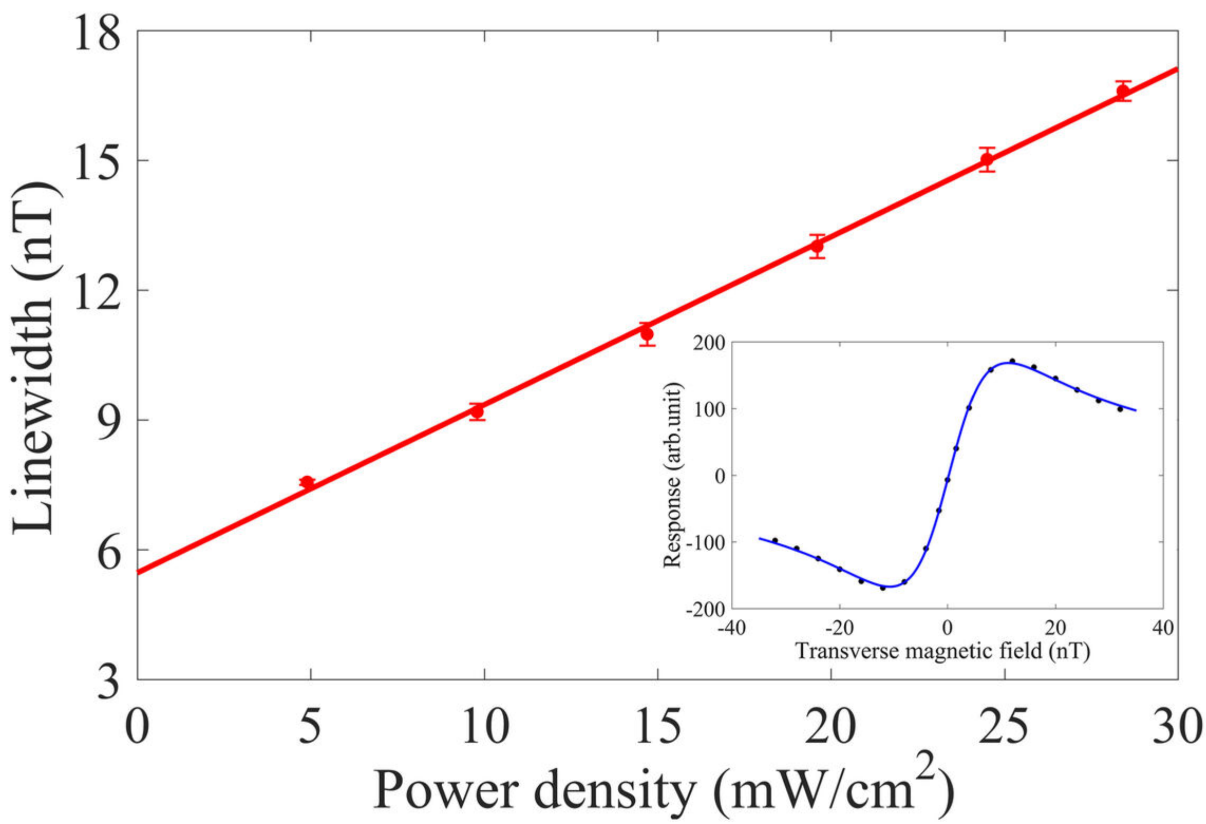
18
15
12
9
6
3
0
5
10
15
20
25
30
Linewidth (nT)
Power density (mW/cm^2)
Response (arb.unit)
200
100
0
-100
-200
-40
-20
0
20
40
Transverse magnetic field (nT)

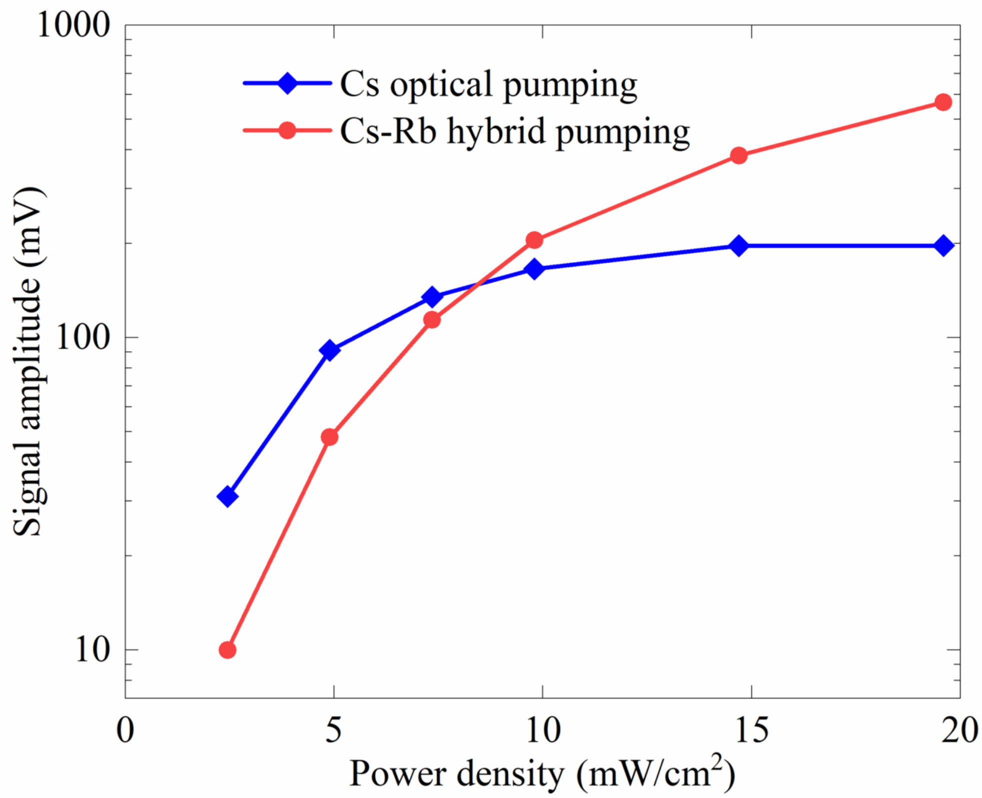
1000
100
10
Signal amplitude (mV)
Cs optical pumping
Cs-Rb hybrid pumping
0
5
10
15
20
Power density (mW/cm2)

PLEASE CITE THIS ARTICLE AS DOI: 10.1063/5.0105945

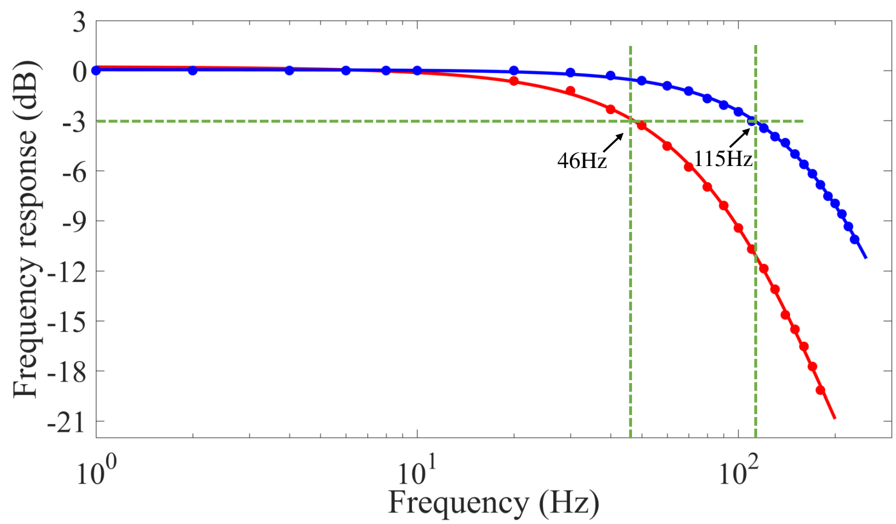

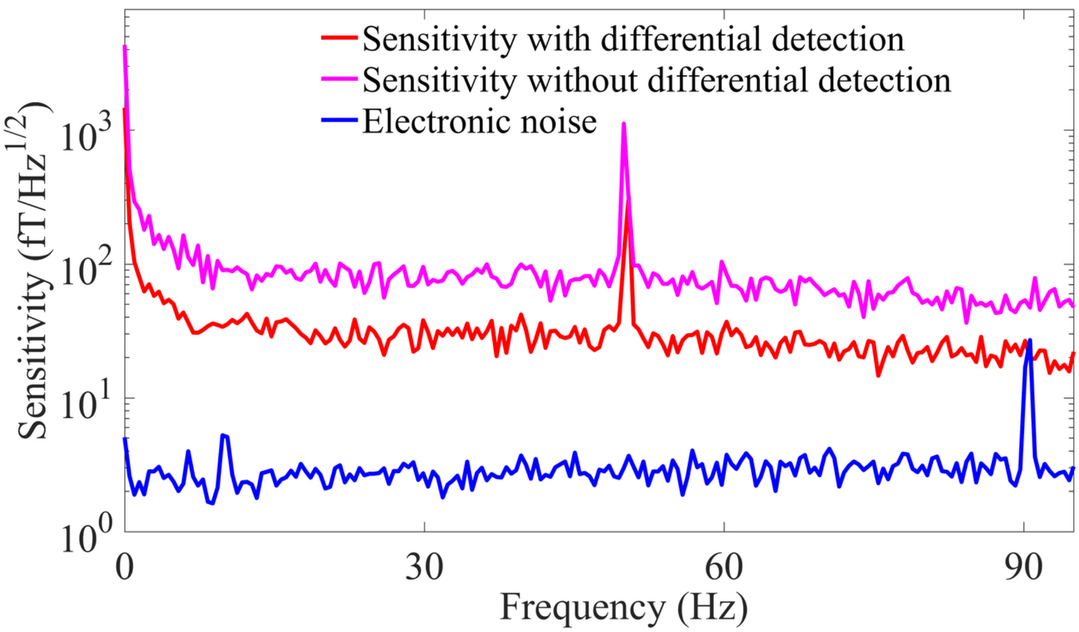
Sensitivity with differential detection
Sensitivity without differential detection
Electronic noise
Sensitivity (fT/Hz$^{1/2}$)
10^0
10^1
10^2
10^3
0
30
60
90
Frequency (Hz)